LIMNOLOGY and OCEANOGRAPHY

ASLO

Limnol. Oceanogr. 68, 2023, 2153–2166

doi: 10.1002/lno.12412

The physiological response of an Antarctic key phytoplankton species to low iron and manganese concentrations

Jenna Balaguer [1,2*] **Silke Thoms,** [2] **Scarlett Trimborn** [2]

[1]Marine Botany, University of Bremen, Bremen, Germany
[2]Ecological Chemistry, Alfred Wegener Institute Helmholtz Centre for Polar and Marine Research, Bremerhaven, Germany

Abstract

Iron (Fe) and manganese (Mn) availability and the divergent requirements of phytoplankton species were recently shown to be potential important drivers of Southern Ocean community composition. Knowledge about Antarctic phytoplankton species requirements for Fe and Mn remains, however, scarce. By performing laboratory experiments and additional calculations of the photosynthetic electron transport, we investigated the response of the ecologically important species *Phaeocystis antarctica* under a combination of different Fe and Mn concentrations. Fe deprivation alone provoked typical physiological characteristics of Fe limitation in *P. antarctica* (e.g., lowered growth and photosynthetic efficiency). In comparison, under Mn deprivation alone, the growth and carbon production of *P. antarctica* were not impacted. Its tolerance to cope with low Mn concentrations resulted from an efficient photoacclimation strategy, including a higher number of active photosystems II through which fewer electrons were transported. This strategy allowed us to maintain similar high growth and carbon production rates as FeMn-enriched cells. Due to its low Mn requirement, *P. antarctica* performed physiologically as Fe-deprived cells under the combined depletion of Fe and Mn. Hence, our study reveals that different from other Southern Ocean phytoplankton species, *P. antarctica* possesses a high capacity to cope with natural low Mn concentrations, which can facilitate its dominance over others, potentially explaining its ecological success across the Southern Ocean.

The Southern Ocean is the world's largest high-nutrient low-chlorophyll (HNLC) region as a result of low concentrations of the trace metal iron (Fe), which acts as a key driver for Antarctic phytoplankton growth and community composition (Martin et al. 1990*a*; Boyd et al. 2007; Sunda 2012). In addition to Fe, total dissolved manganese (Mn) concentrations were also found to be low in the Atlantic sector (0.04 nmol L^{-1}; Middag et al. 2011) and in several other regions of the Southern Ocean, such as the Weddell Sea (< 0.2 nmol L^{-1}; Middag et al. 2013), Ross Sea (0.21–0.26 nmol L^{-1}; Wu et al. 2019), and the Drake Passage (≈ 0.03–2 nmol L^{-1}; Middag et al. 2012; Browning et al. 2014, 2021; Balaguer et al. 2022). Already in the early 1990s, low Mn concentrations were reported in the Drake Passage, which led John Martin and colleagues to hypothesize the importance of Mn next to Fe for phytoplanktonic growth (Martin et al. 1990*b*).

Indeed, Fe and Mn are essential elements required for cell growth. Fe is needed in many cell pathways, including photosynthesis and respiration processes, nitrogen fixation, and chlorophyll synthesis (Behrenfeld and Milligan 2013; Twining and Baines 2013). Mn is the second most abundant trace metal required in the thylakoids (Raven et al. 1999), being an essential element of the metalloenzyme cluster of the oxygen-evolving complex during photosynthesis (Raven 1990). It is also requisite for the antioxidant enzyme superoxide dismutase to scavenge reactive oxygen species during photosynthesis (Wolfe-Simon et al. 2005). Both superoxide dismutase and photosystem II have a high Mn demand (Raven 1990; Yu and Rengel 1999). Accordingly, Mn was unraveled to limit alone or to co-limit with Fe Southern Ocean phytoplankton biomass buildup based on various FeMn-enrichment incubation experiments in the Drake Passage (Browning et al. 2014, 2021; Balaguer et al. 2022), Weddell Sea (Buma et al. 1991), and Ross Sea (Wu et al. 2019), and more recently projected in a biogeochemical model (Hawco et al. 2022). Within the same Southern Ocean phytoplankton community, it was also uncovered that the growth of the most

*Correspondence: jenna.balaguer@awi.de

Additional Supporting Information may be found in the online version of this article.

Author Contribution Statement: J.B. acquired and analyzed the presented data. J.B. and S.Tr. designed the study and interpreted the data. S.Th. performed the model analyses. J.B. wrote the manuscript with critical feedback from S.Tr. and S.Th.

abundant diatom *Fragilariopsis* sp. was FeMn co-limited. In contrast, the other diatoms of the community were primarily Fe-limited (Balaguer et al. 2022). In addition, in a monocultural laboratory experiment, the Antarctic diatom *Chaetoceros debilis* was found to be FeMn co-limited when grown under FeMn-poor natural seawater (Pausch et al. 2019).

Next to diatoms, the haptophyte *Phaeocystis* usually thrives across the Southern Ocean (Weddell Sea, Ross Sea, and the Drake Passage; *see* review Schoemann et al. 2005). *Phaeocystis antarctica* is a major actor in carbon fixation (DiTullio et al. 2000), and due to its unique physiology (Lancelot et al. 1994), it has an essential role in ocean biogeochemistry (Schoemann et al. 2005). The ubiquitous *P. antarctica* is mainly observed during spring and summer (Stoecker et al. 1995) as well as in seasonal ice zones and coastal waters (El-Sayed et al. 1983). While it is well documented that *P. antarctica* can cope with Fe limitation by adjusting its pigment composition (van Leeuwe and Stefels 1998; DiTullio et al. 2007), photophysiology (van Leeuwe and Stefels 2007; Alderkamp et al. 2012; Strzepek et al. 2012), and elemental stoichiometry (Koch et al. 2019; Trimborn et al. 2019), co-limitation of *P. antarctica* with another trace metal is, however, less understood. According to a recent laboratory study, the colonial *P. antarctica* exhibited reduced photosynthetic efficiency under Mn depletion and altered expression of specific protein signatures (e.g., flavodoxin and plastocyanin) when both Fe and Mn supplies were low, suggesting Mn deficiency in this species under low light (25 μmol photons m^{-2} s^{-1}; Wu et al. 2019). Due to its complex life cycle (Schoemann et al. 2005), whether this is also the case for the solitary *P. antarctica* remains unknown. To fill this gap, we conducted a laboratory experiment and performed cellular modeling of the photosynthetic electron transport to understand the photophysiological adjustments and trace metals requirements of *P. antarctica* under low natural Fe and/or Mn concentrations representative of natural Southern Ocean waters.

Methods

Experimental setup

The experiment was performed with the solitary *P. antarctica* (solitary cells isolated by P. Pendoley in March 1992 at 68°39′S, 72°21′E). *P. antarctica* was pre-acclimated for at least 10 generations and was grown for the main experiment in 0.2 μm filter-sterilized (0.2 μm, Sartobran, Sartorius) naturally FeMn-poor Antarctic seawater (Table 1) under trace metals clean conditions. The water was sampled from 25 m depth during Polarstern expedition PS112 at 62.2S–64.6W in 2018. This seawater was spiked with chelexed (Chelex 100; Sigma-Aldrich) macronutrients (100 μmol L^{-1} Si, 100 μmol L^{-1} NO_3^-, and 6.25 μmol L^{-1} PO_4^{3-}) and vitamins (30 nmol L^{-1} B_1, 23 nmol L^{-1} B_7, and 0.228 nmol L^{-1} B_{12}) according to $F/2_R$ medium (Guillard and Ryther 1962). To represent trace metal concentrations of Southern Ocean HNLC waters, a mixture of zinc (0.16 nmol L^{-1}), copper (0.08 nmol L^{-1}), cobalt (0.09 nmol L^{-1}), molybdenum (0.05 nmol L^{-1}) was added and adjusted to maintain the ratio of the original $F/2_R$ recipe. The different treatments consisted of four different concentrations of Fe and Mn to the culture medium, where Fe and Mn were added as iron chloride ($FeCl_3$, 2.8 nmol L^{-1}, AAS standard, TraceCERT, Fluka) and manganese chloride ($MnCl_2$, 2.8 nmol L^{-1}, AAS standard, TraceCERT, Fluka):

Table 1. Dissolved and intracellular concentrations of trace metals. At the end of the experiment, total dissolved Fe, Mn, Zn, and the deficiency of dissolved Mn relative to Fe concentrations (Mn*, *see* Methods; Eq. 2) were determined in the culture medium (without cells) and in the *Phaeocystis antarctica* incubation bottles after exposure to different Fe and Mn availabilities. Intracellular Fe and Mn contents of *P. antarctica* were also determined at the end of the experiment. Values represent the mean ± SD (Culture medium dissolved Fe: $n = 2$, Culture medium dissolved Mn–Zn: $n = 4$, *P. antarctica* incubations dissolved Fe: $n = 6$, *P. antarctica* incubations dissolved Mn–Zn: $n = 6$, Intracellular TM content of *P. antarctica*: $n = 3$). Different letters from a to c indicate significant differences from the highest to the lowest mean ($p < 0.05$). nd Denotes that values could not be determined.

Parameter	Control	−Mn	−Fe	−FeMn
Culture medium				
Dissolved Fe (nmol L^{-1})	2.15	1.88	0.27	0.63
Dissolved Mn (nmol L^{-1})	2.70±0.18a	0.15±0.02b	2.71±0.07a	0.13±0.03b
Dissolved Zn (nmol L^{-1})	10.49±nd	9.33±0.66	9.41±0.56	9.17±1.26
Mn* (nmol L^{-1})	1.89	−0.55	2.61	−0.11
P. antarctica incubations				
Dissolved Fe (nmol L^{-1})	0.71±0.02a	1.02±0.12a	0.33±nd	0.23±nd
Dissolved Mn (nmol L^{-1})	1.31±0.06a	0.00±0.00b	1.63±0.49a	0.02±0.01b
Dissolved Zn (nmol L^{-1})	6.13±0.21a	5.47±0.45a	6.38±0.57a	6.89±0.91a
Intracellular TM content of *P. antarctica*				
Fe (amol Fe $cell^{-1}$)	4.20±0.90a	4.60±0.53a	3.36±0.56ab	1.44±1.68b
Mn (amol Mn $cell^{-1}$)	0.59±0.18a	0.23±0.09b	0.36±0.15ab	0.23±0.06b

[Correction added on 18th August 2023, after first online publication: Table 1 values and Equation 2 has been updated in this version.]

enriched either with both Fe and Mn (*Control treatment*), with Fe alone (*−Mn treatment*), with Mn alone (*−Fe treatment*), and no addition (*−FeMn treatment*) (Table 1). To all culture media, no addition of ethylenediaminetetraacetic acid was made to reduce the alteration of the natural seawater trace metal chemistry and ligands (Gerringa et al. 2000). Due to an initial Fe complexing capacity of 1.32 ± 0.29 nmol L^{-1}, it is supposed that most of the added Fe were buffered rather than forming inorganic colloids. To contain contamination, trace metal clean techniques (sampling and handling) were used during the whole experiment. All incubation bottles and other equipment needed for the experiment were cleaned 7 d in a detergent bath containing 1% Citranox solution (Sigma-Aldrich) followed by rinsing seven times with Milli-Q (Millipore). Then, they have been subsequently filled with 1 mol L^{-1} hydrochloric acid for 7 d. After seven rinsing steps with Milli-Q, all types of equipment were dried under a clean bench (Class 100; Opta) and stored triple-bagged in polyethylene bags until usage. All *P. antarctica* cells were kept in mid-exponential growth in dilute batch cultures and were grown in triplicates in polycarbonate bottles, in 1 L bottles during the acclimation phase, and in 4 L bottles during the main experiment. The initial inoculum for each treatment was ≈ 2500 cells mL^{-1}, and each treatment was harvested when cells had reached a density between 80,000 and 150,000 cells mL^{-1}. The main experiment lasted between 9 and 11 d, depending on the experimental treatment. Each incubation was grown at 100 μmol photons m^{-2} s^{-1} under a 16 : 8 (light : dark) hours cycle at 2°C. As the strain of *P. antarctica* used for the experiment does not form colonies, the cell density and size were monitored every 2 d using a Beckman Multisizer™ 3 Coulter Counter® with a 100 μm aperture.

The maximum growth rate (μ, d^{-1}) was determined from Eq. 1:

$$\mu = \frac{\ln(Nt_2/Nt_1)}{\Delta t}, \quad (1)$$

where N_{t1} and N_{t2} are the cell abundance at the start (day 3 or 5 depending on the treatment) and the end (day 9 or 11 depending on the treatment) of the experimental phase of growth (Supporting Information Fig. S1), respectively, while Δt is the duration of the exponential growth phase, in days.

To ensure that *P. antarctica* was not forming colonies, the cultures were also monitored unfixed and fixed with Lugol's solution via light microscopy at the beginning, during, and at the end of the experiments. Briefly, samples were fixed with Lugol's solution (1% final concentration) and stored at 2°C in the dark until analysis. All samples were allowed to settle in Utermöhl sedimentation chambers (Hydrobios) for at least 24 h and were analyzed on an inverted light microscope (Axiovert 200; Zeiss), according to the method of Utermöhl (1958).

Trace metal seawater chemistry

Total dissolved Fe and Mn concentrations were determined in the culture medium (without cells) (Table 1). To this end, 100 mL of seawater was filtered through hydrochloric acid-cleaned polycarbonate filters (0.2 μm pore size; EMD Millipore) using a trace metal clean filtration system, and the filtrate collected in a hydrochloric acid-cleaned polyethylene bottle, which was stored triple bagged at 2°C for immediate analysis. Concentrations of total dissolved Fe and Mn were analyzed via external calibration using a SeaFast system (Elemental Scientific) coupled to an inductive plasma mass spectrometer (Element2; Thermo Fisher Scientific, resolution of 2000) (Hathorne et al. 2012; Rapp et al. 2017). An iminodiacetate chelation column (part number CF-N-0200; Elemental Scientific) was used during the preconcentration step. Before analysis, all seawater samples were acidified to pH 1.7 with a double distilled nitric acid (distilled 65%, pro analysis; Merck) and irradiated for 1.5 h using a UV power supply system (7830) and photochemical lamp (7825) from ArcGlass to provide total dissolved concentrations of trace metals and avoid the presence of organic compounds (Biller and Bruland 2012). During each UV digestion step, two blanks were performed. The inductive plasma mass spectrometer was optimized daily to achieve oxide forming rates below 0.3%. Each seawater sample was analyzed via standard addition to minimize any matrix effects that might influence the quality of the analysis. To assess the accuracy and precision of the method, a NASS-7 (National Research Council of Canada) reference standard was analyzed in a 1 : 10 dilution (corresponding to environmentally representative concentrations) at the beginning, in the middle, and at the end of a run (two batch runs; $n = 18$). Recoveries for Fe and Mn were 104%. The measured values were within the limits of the certified NASS-7 reference material with a concentration of 6.5 ± 0.02 nmol L^{-1} for dissolved Fe and 14.2 ± 0.17 nmol L^{-1} for dissolved Mn.

The Mn deficiency rate (Mn*, nmol L^{-1}) was determined from Eq. 2 (Browning et al. 2021):

$$\mathrm{Mn}^* = d\mathrm{Mn} - d\mathrm{Fe}/R, \quad (2)$$

where R is the assumed average of the phytoplankton Fe : Mn ratio (2.67; Moore et al. 2013).

Elemental composition and stoichiometry

Particulate organic carbon and nitrogen

At the end of the experiment, 250 mL of water was filtered onto precombusted glass-fiber filters (15 h, 500°C, GF/F, ≈ 0.6 μm, 25 mm; Whatman) and stored at −20°C in precombusted glass Petri dishes. Before analysis with a Euro Elemental Analyzer 3000 CHNS-O (HEKAtech GmbH), the filters were dried for > 12 h at 60°C and then acidified with 200 μL of 0.2 N hydrochloric acid to remove inorganic carbon and dried a second time. Contents of particulate organic carbon (POC) and particulate organic nitrogen (PON) were corrected for blank measurements and normalized to filtered volume and cell densities to yield cellular quotas. The POC production rate (pg C $cell^{-1}$ d^{-1}) was determined from Eq. 3:

$$POC_{production} = POC_{content} \times \mu, \quad (3)$$

where μ is the maximum growth rate (Eq. 1).

Cellular trace metals quotas

For determination of the cellular trace metal content, at the end of the experiment, 400 mL of water was filtered onto 0.2 μm trace metal cleaned polycarbonate filters (EMD Millipore) and then rinsed for 15 min with a 0.1 mol L^{-1} oxalic acid wash to remove cell surface bound trace metals (Hassler and Schoemann 2009). Finally, the filters were rinsed with filtered seawater and stored in 5 mL trace metal-cleaned polyfluoroalkyl vials until further analysis. Samples were analyzed with an inductive plasma mass spectrometer following digestion with nitric and hydrofluoric acid (Ho et al. 2003; Twining and Baines 2013; Koch et al. 2019). The filters were digested for 16 h at 180°C using 5 mL of sub-boiled nitric acid and 0.5 mL of sub-boiled hydrofluoric acid (40%, suprapure; Merck) followed by the addition of 0.5 mL of Milli-Q water.

Via evaporation using a 140°C hot plate, the volume of the cell extract was concentrated down to 0.5 mL and the evaporate was then passed through a calcium/sodium hydroxide solution. Then, 0.2 mL of sub-boiled nitric acid was added as an internal standard diluted up to 10 mL with Milli-Q water and analyzed on a high-resolution inductive plasma mass spectrometer (Attom; Nu Instruments). To avoid high background trace metal concentrations and to ensure high digestion quality, acid (5 mL of sub-boiled nitric acid and 0.5 mL hydrofluoric acid), two filter blanks, as well as the BCR-414 (Plankton reference material; Sigma-Aldrich) samples were also processed and analyzed (Supporting Information Table S1). Intracellular trace metal contents were normalized to filtered volume, cell densities, and POC.

Pigments

At the end of the experiment, 250 mL of sample were filtered onto 0.2 μm filters (25 mm, GFF; Whatman) and directly flashed frozen into liquid nitrogen. The samples were stored at −80°C in the dark until further analysis. The concentrations of the light-harvesting (LH) pigments chlorophyll *a* and c_2, fucoxanthin, and the light protective (LP) pigments diatoxanthin and diadinoxanthin were determined by reverse-phase high-performance liquid chromatography after centrifugation (5 min, 4°C, 13000 rpm) and filtration through a 0.45 μm pore size nylon syringe filter (Nalgene®; Nalge Nunc International) (Wright et al. 1991). LaChromElite® system was used to run the analysis. For pigments separation, a Spherisorb® ODS-2 column (25 cm × 4.6 mm, 5 μm particle size; Waters) with a LiChropher® 100-RP-18 guard cartridge was used, and the gradient was applied according to Wright et al. (1991). Using the software EZChrom Elite ver. 3.1.3. (Agilent Technologies), the peaks were detected at 440 nm and then identified and quantified by co-chromatography with standards for chlorophyll *a*, chlorophyll c_2, fucoxanthin, diatoxanthin, and diadinoxanthin (DHI Lab Products). Pigment contents were normalized to filtered volume and cell densities.

Photophysiology

Chlorophyll *a* fluorescence measurements were performed using a Fast Repetition Rate fluorometer coupled to a FastAct Laboratory system (FastOcean PTX, both from Chelsea Technologies Group). The measurements were performed at the start, during, and at the end of the experiment. The excitation wavelengths of the fluorometer's LEDs were 450, 530, and 624 nm, and the light intensity was automatically adjusted between 0.66–1.2 × 10^{22} photons m^{-2} s^{-1}. The single turnover mode was set with a saturation phase of 100 flashlets on a 2 μs pitch followed by a relaxing phase of 40 flashlets on a 50 μs pitch. To calculate the maximum quantum yield of photosystem II F_v/F_m (dimensionless), the minimum (F_0) and maximum (F_m) chlorophyll *a* fluorescence was determined after 10 min of dark acclimation (Eq. 4) (Oxborough and Baker 1997):

$$F_v/F_m = (F_m - F_0)/F_m, \quad (4)$$

with the F_v/F_m measured before and after the fluorescence light curve, the F_v/F_m recovery was calculated and expressed as a % of the initial F_v/F_m.

The functional absorption cross-section of photosystem II (σ_{PSII}, nm^2), the time constant for electron transport at the acceptor side of photosystem II (τ_{Qa}, μs), the concentration of functional photosystem II reaction centers ([RCII], zmol $cell^{-1}$), the connectivity factor (P, dimensionless) and the non-photochemical quenching (Supporting Information Fig. S2) were derived using the FastPro8 Software (Version 1.0.55; Kevin Oxborough, CTG Ltd) from Oxborough et al. (2012). Electron transport rates (ETRs) irradiance curves were conducted by applying 8 irradiances from 0 up to ≈ 800 μmol photons m^{-2} s^{-1} for 5 min for each light level at the end of the experiment. A light sensor (ULM-500; Walz GmbH) measured each light intensity (E, μmol photons m^{-2} s^{-1}) emitted from the FastAct Laboratory system. Using the following formula, ETRs (e^- $PSII^{-1}$ s^{-1}) were derived according to Suggett et al. (2004, 2009) (Eq. 5):

$$ETR = \sigma_{PSII} \times \frac{(F_q'/F_m')}{(F_v/F_m)} \times E, \quad (5)$$

where F_q'/F_m' is the effective photosystem II quantum yield at ambient light. Maximum ETR (ETR, e^- $PSII^{-1}$ s^{-1}), light utilization efficiency (α), and minimum saturating irradiance (I_K, μmol photons m^{-2} s^{-1}) were calculated from the fitted irradiance-dependent ETR using the model of Platt et al. (1981) (Silsbe and Kromkamp 2012) through a Nelder–Mead method programmed on R Studio (version 1.1.463, © 2009–2016). The overall ETR per cell (ETR_{cell}) was derived as a multiplication of the photosystem II normalized ETR with [RCII].

Modeling

The cell model used in this study was adapted from Kroon and Thoms (2006). This model aims to describe phytoplankton steady-state growth by including the main mechanisms and processes in photosynthetic electron transport, involving all intermediary steps from photon absorption and charge separation at photosystem II up to the reduction of the terminal electron carrier ferredoxin at the end of the electron transport chain. In particular, the model includes the representation of a free plastoquinone pool interacting with a Q_B binding site at photosystem II, the cytochrome b6/f complex, the Q-cycle, the binding of ferredoxin to the cytochrome b6/f (which allows for cyclic electron transport) and the electron transfer steps within photosystem I. The model describes photosynthesis in terms of electron flow, which is assumed to be the most elementary product for describing the consequences of different Fe-deficient and Mn-deficient treatments on well-known growth characteristics (e.g. ETR curve). As a result of the photochemical nature of the model, ETR normalized to photosystem II and ETR of the entire *P. antarctica* cells were calculated (Fig. 4), please note that the model outputs are represented by lines-connected points and were not fitted. The used parameters of the model by Kroon and Thoms (2006) adapted to *P. antarctica* are shown in Supporting Information Table S2.

Statistics

Shapiro–Wilk tests were performed to test the normal distribution and equal variances of the data set. A one-way analysis of variance was conducted to assess the impact of Fe and Mn concentrations on the different parameters. As post hoc tests, the Tukey honest significant difference test was used between the mean groups. Significant differences among treatments were established at a $p < 0.05$ level indicated by letters. Different letters indicate significant differences at the 5% level from the higher mean (a) to the lowest mean (c). All statistical analyses were performed with R Studio (version 1.4.1106, © 2009–2021). R packages to reproduce statistical analysis are: stats (aov and lm functions) and agricolae (HSD.test function).

Results

Trace metal chemistry

The concentration of total dissolved Fe in the culture medium (without *P. antarctica* cells) was higher in the Control and the −Mn treatments (≈ 2 nmoL L^{-1}; Table 1) relative to the −Fe and −FeMn treatments (≤ 0.6 nmoL L^{-1}; Table 1). In comparison, the concentration of the total dissolved Mn in the culture medium (without *P. antarctica* cells) was significantly ($p < 0.05$) higher in the Control and the −Fe treatments relative to the −Mn and −FeMn treatments (Table 1). At the end of the experiment, the concentrations of total dissolved Fe in the culture medium (with *P. antarctica* cells) were lower in all Fe-poor treatments (−Fe and −FeMn) compared to the Control and remained similar between the −Mn and the Control treatment. The concentrations of total dissolved Fe in the culture medium (with *P. antarctica* cells) were lower in all Mn-poor treatments (−Mn and −FeMn) compared to the Control and remained similar between the −Fe and the Control. The deficiencies of dissolved Mn relative to Fe concentrations (Mn*, *see* Methods; Eq. 2) were the lowest in the Mn-deficient treatments (−0.55 and −0.11 nmol L^{-1} for −Mn and −FeMn, respectively) and the highest in the Fe-deficient treatment (2.61 nmol L^{-1}) compared to the Control. The concentration of total dissolved zinc (Zn) in the culture medium (without and with *P. antarctica* cells) remained similar across all treatments (Table 1).

Growth and elemental composition

The growth rate of *P. antarctica* in the Control treatment was similar to the one in the −Mn treatment (Fig. 1a). Compared to the Control, the growth rate was significantly ($p < 0.05$) decreased in both Fe-poor treatments (−Fe: 8% and −FeMn: 5%). For all treatments, the size of the *P. antarctica* cells remained similar, being ≈ 3.2 μm (Supporting Information Table S3). Under every experimental condition, the particulate organic carbon (POC) content of *P. antarctica* remained the same (≈ 4 pg $cell^{-1}$; Fig. 1b). The POC production rates of both low Fe supply treatments (−Fe and −FeMn) were significantly ($p < 0.05$) decreased by ≈ 15% relative to the −Mn treatment (Fig. 1c). The molar carbon : nitrogen ratios (C : N; Fig. 1d), as well as the PON contents (Supporting Information Fig. S3), were not altered under all experimental conditions. Compared to the Control, the molar TM : C ratio of *P. antarctica* in the −FeMn treatment decreased significantly ($p < 0.05$) by ≈ 70% for Fe (Fig. 2a) and by ≈ 60% for Mn (Fig. 2b). In addition, low Mn concentrations alone (−Mn) also significantly ($p < 0.05$) decreased the Mn : C ratio by 60% when compared to the Control (Fig. 2b).

Photophysiological response

Compared to the Control, the dark-adapted maximum quantum yield of photosystem II (F_v/F_m) of all other treatments was significantly decreased ($p < 0.05$), with a decrease by ≈ 10% in the −Fe and by ≈ 20% in the two Mn-deficient treatments (−Mn, −FeMn) (Table 2). The functional absorption cross-sections of photosystem II (σ_{PSII}) of the −Mn remained unchanged relative to the Control (Table 2). Adversely, σ_{PSII} of both Fe low supply treatments (−Fe and −FeMn) increased by 34% and 50%, respectively, compared to the Control (Table 2). The time constant for electron transfer at photosystem II (τ_{Qa}) remained unchanged between Control and −Mn but decreased by 12% in response to Fe depletion alone and more strongly by ≈ 20% under a low supply of both Fe and Mn (Table 2). The connectivity between adjacent photosystems (P) decreased similarly by ≈ 30% for all other treatments compared to the Control (Table 2). Relative to the Control, the concentration of functional photosystem II reaction centers [RCII] was significantly ($p < 0.05$) increased in all

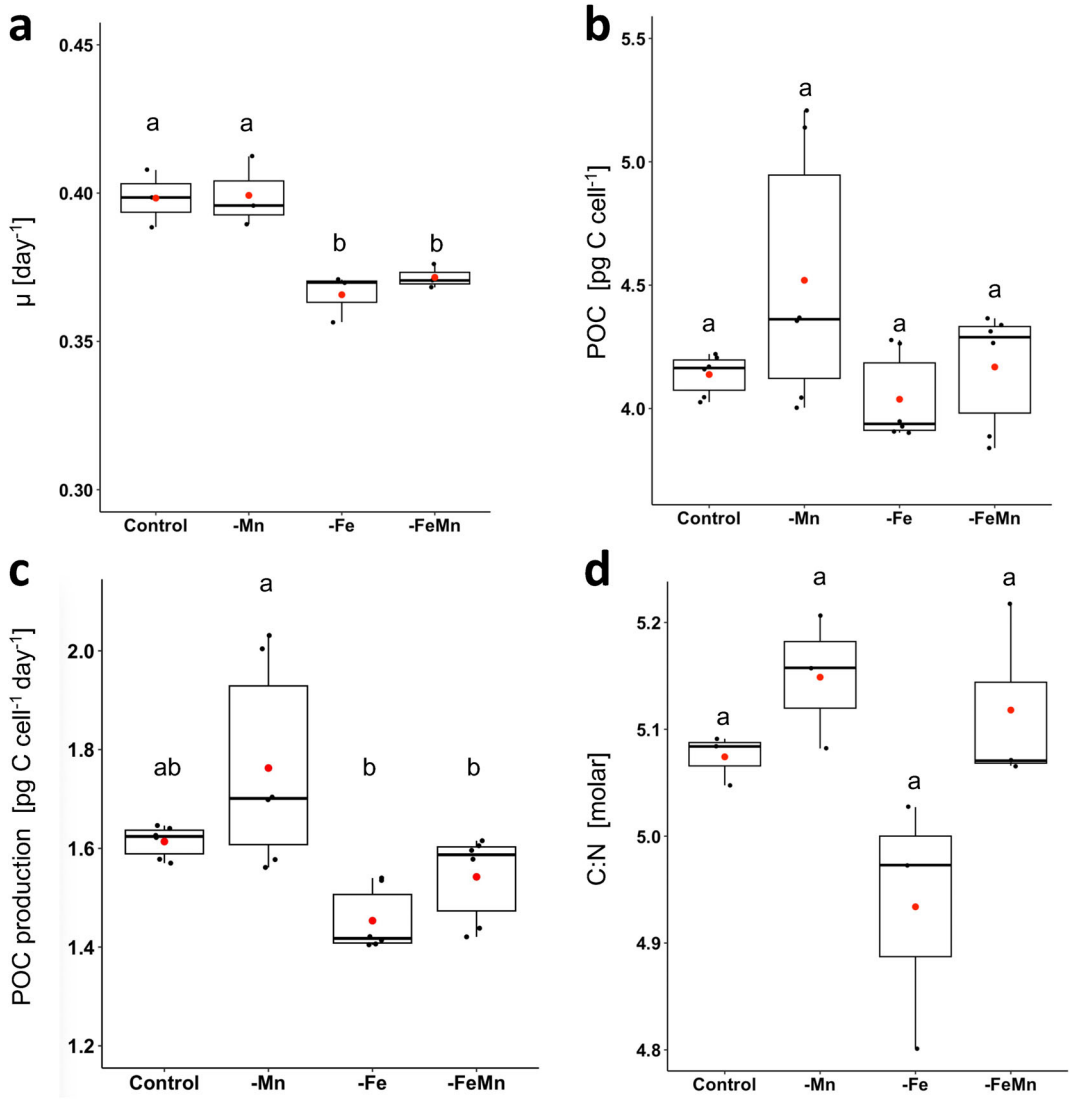

Fig. 1. Growth and elemental composition of *Phaeocystis antarctica*. Box plots of growth rate μ (**a**), content of particulate organic carbon (POC) (**b**), daily production rate of POC (**c**), and molar carbon : nitrogen ratio (C : N) (**d**) were determined in cells grown under different Fe and Mn availabilities at the end of the experiment. The black points represent the individual replicates, and the red points represent the mean. Different letters from a to c indicate significant differences from the highest to the lowest mean ($p < 0.05$).

other treatments (−Mn: 22%, −Fe: 13% and −FeMn: 18%; Table 2). Compared to the Control, the F_v/F_m recovery of all other treatments significantly ($p < 0.05$) decreased between 10% and 20%, with no differences across these treatments (−Mn, −Fe, and −FeMn; Table 2). The −FeMn treatment reached the highest ETR values relative to the other treatments (Fig. 3; Table 2). Relative to the Control, the ETR_{max} was strongly increased by 13% and 51% in the −Fe and −FeMn treatments, respectively (Table 2). Adversely, only when grown under −Mn, ETR significantly ($p < 0.05$) decreased by 20% relative to the Control (Figs. 3, 4a; Table 2). In comparison, ETRs of a single *P. antarctica* cell (ETR_{cell}) remained unchanged in Control and −Mn treatments (Fig. 4b). The minimum saturating irradiance (I_k) was similar across all treatments ($\approx 50\ \mu$mol photons $m^{-2}\ s^{-1}$; Table 2). The light use efficiencies (α) of the Control, −Mn, and −Fe treatments were similar but significantly ($p < 0.05$) increased in the −FeMn treatment (Table 2).

Pigment composition

The concentration of the LP pigments (LP = sum of diadinoxanthin and diatoxanthin; Table 3) was similar in the Control and the −Mn treatment (Table 3). Only when Fe supply was low (−Fe and −FeMn) the concentration of LP significantly ($p < 0.05$) decreased by 31% and 24%, respectively, relative to the Control, primarily due to the reduction of

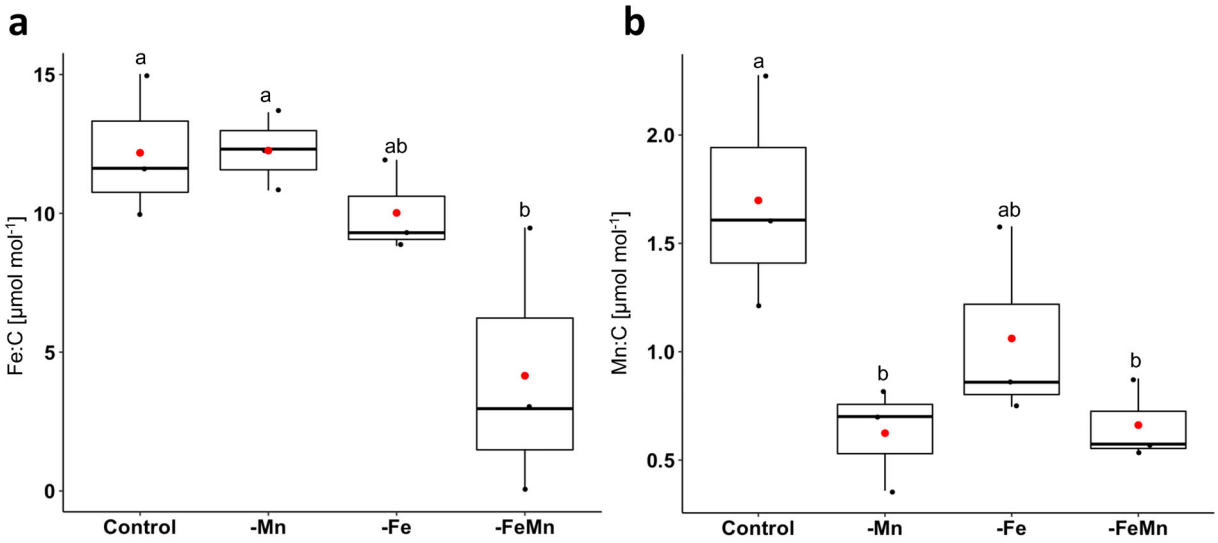

Fig. 2. Molar trace metal to carbon ratio of *Phaeocystis antarctica*. Box plots of Fe : C ratio (**a**) and Mn : C ratio (**b**) were determined in cells grown under different Fe and Mn availabilities at the end of the experiment. The black points represent the individual replicates, and the red points represent the mean. Different letters from a to c indicate significant differences from the highest to the lowest mean ($p < 0.05$).

Table 2. Photophysiological responses. The dark-adapted maximum quantum yield (F_v/F_m), the functional absorption cross-section of photosystem II (σ_{PSII}), the time constant for electron transfer at photosystem II (τ_{Qa}), the connectivity between adjacent photosystems (P), the concentration of functional reaction centers for photosystem II ([RCII]), the F_v/F_m recovery, the minimum saturating irradiance (I_k), light utilization efficiency (α) and the maximum electron transport rate (ETR_{max}) were determined after exposure to different Fe and Mn availabilities at the end of the experiment. Values represent the mean ± SD ($n = 3$). Different letters from a to c indicate significant differences from the highest to the lowest mean ($p < 0.05$).

Parameter	Control	−Mn	−Fe	−FeMn
F_v/F_m (dimensionless)	0.36±0.01a	0.29±0.02c	0.32±0.01b	0.29±0.02c
σ_{PSII} (nm^2)	6.2±0.6c	6.6±0.7c	8.3±0.7b	9.3±2.8a
τ_{Qa} (μs)	779±92a	814±83a	683±51b	628±73c
P (dimensionless)	0.25±0.08a	0.18±0.06b	0.17±0.07b	0.16±0.07b
[RCII] (zmol $cell^{-1}$)	23±3b	28±3a	26±2a	27±2a
F_v/F_m recovery (%)	67±1a	56±3b	54±0b	60±3b
ETR_{max} (e^- $PSII^{-1}$ s^{-1})	275±13b	222±25c	312±28b	416±17a
I_k (μmol photons m^{-2} s^{-1})	54±27a	50±24a	51±30a	56±29a
α (dimensionless)	5.0±0.5b	4.5±0.6b	6.1±0.9ab	7.4±0.6a

Table 3. Pigment concentrations. The concentration of chlorophyll *a*, chlorophyll c_2, fucoxanthin, diadinoxanthin, diatoxanthin, light protective pigments (LP = diadinoxanthin + diatoxanthin), and the light-harvesting pigments (LH = chlorophyll *a* + chlorophyll c_2 + fucoxanthin) were determined after exposure to different Fe and Mn availabilities at the end of the experiment. Values represent the mean ± SD ($n = 3$). Different letters from a to c indicate significant differences from the highest to the lowest mean ($p < 0.05$).

Parameter	Control	−Mn	−Fe	−FeMn
Chlorophyll *a* (fg $cell^{-1}$)	49±3ab	59±9a	43±3b	43±3b
Chlorophyll c_2 (fg $cell^{-1}$)	11±1a	13±2a	11±0.4a	11±0.4a
Fucoxanthin (fg $cell^{-1}$)	19±1b	28±4a	13±3b	12±3b
Diadinoxanthin (fg $cell^{-1}$)	11±1a	11±2ab	8±0.4c	9±0.1bc
Diatoxanthin (fg $cell^{-1}$)	0.9±0.1a	0.5±0.02b	0.5±0.02b	0.4±0.2b
LP (fg $cell^{-1}$)	12.31±0.99a	11.72±1.64ab	8.49±0.40c	9.31±0.13bc
LH (fg $cell^{-1}$)	78.54±5.24ab	100.56±14.78a	67.15±5.51b	66.25±6.74b

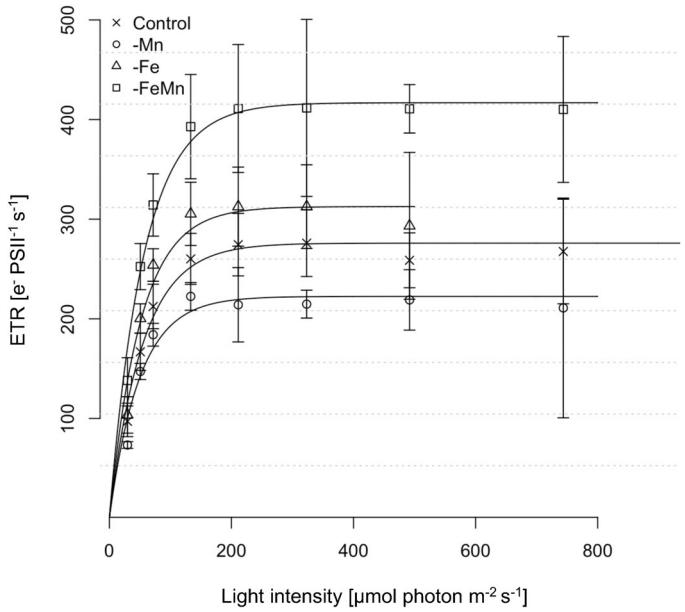

Fig. 3. Electron transport rates (ETRs) vs. light intensity. ETRs were measured in response to increasing light intensity in *Phaeocystis antarctica* after exposure to different Fe and Mn availabilities at the end of the experiment. Values represent the mean ± SD ($n = 3$).

diadinoxanthin concentrations (Table 3). The concentration of the LH pigments (LH = sum of chlorophyll *a*, chlorophyll c_2, and fucoxanthin; Table 3) remained the same for the treatments −Mn, −Fe, and −FeMn compared to the Control (Table 3). However, fucoxanthin concentration significantly increased only when Mn supply was low (−Mn; Table 3).

Discussion

To understand how low Fe and Mn concentrations affect Southern Ocean phytoplankton community composition, laboratory studies provide insight into their physiological strategies, which may explain why some species occur in a specific location and others do not. Due to a limited knowledge of the species-specific Fe and Mn requirements of Southern Ocean phytoplankton species, we conducted a FeMn addition experiment with the ecologically important *P. antarctica* and provide a modeling-based interpretation of the photophysiological data. While *P. antarctica* was Fe limited, it was not by low Mn supply due to its low Mn requirements.

P. antarctica was not limited by low Mn supply

Based on previous laboratory experiments, Mn deficiency resulted in a reduced rate of growth accompanied by a decreased rate of POC production for several temperate (Sunda and Huntsman 1983; Peers and Price 2004) and an Antarctic diatom (Pausch et al. 2019). In contrast, this was not the case for our tested species (−Mn treatment; Fig. 1a,c) as *P. antarctica* was not affected by the applied low Mn concentration (0.15 ± 0.02 nmol L^{-1}; Table 1). These results are consistent with previous observations of another *P. antarctica* strain, which was grown in Mn-free artificial seawater in the laboratory (Wu et al. 2019). Moreover, the dissolved Mn concentration of our −Mn treatment is representative of previously measured dissolved Mn values in several areas of the Southern Ocean (≤ 0.2 nmol L^{-1}), such as the Atlantic sector (Middag et al. 2011), the Weddell Sea (Middag et al. 2013), the Ross Sea (Wu et al. 2019), and the Drake Passage

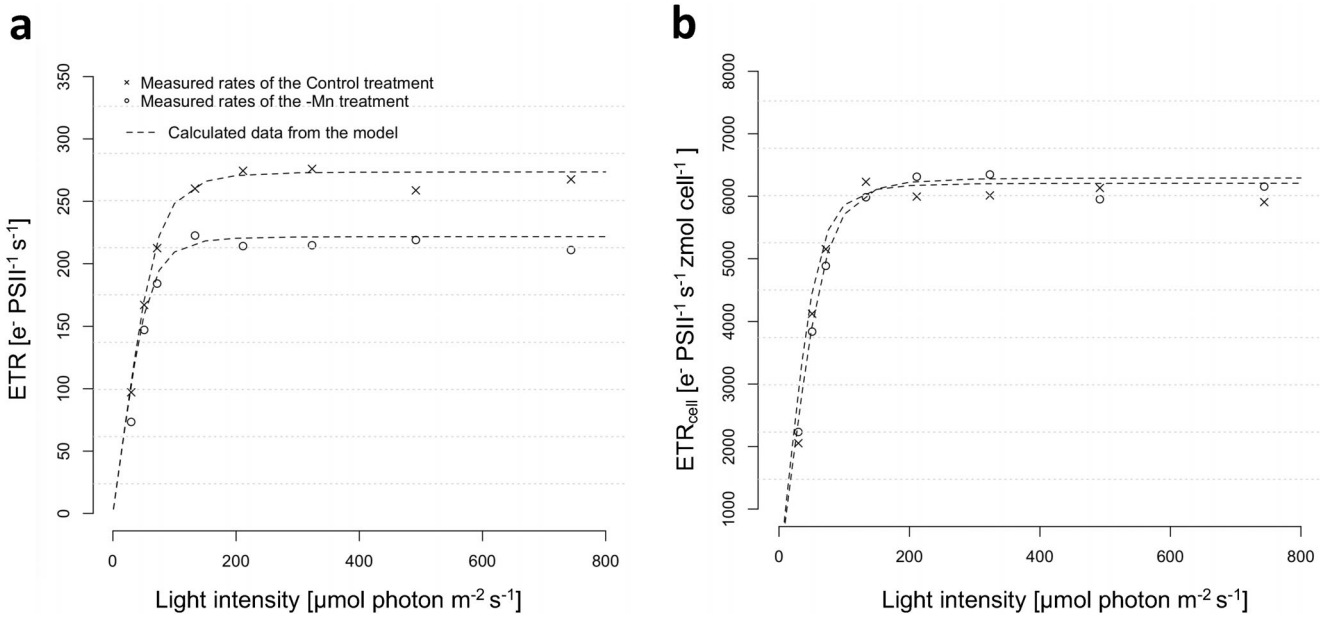

Fig. 4. Measured and calculated electron transport rates normalized to either photosystem II (ETR) (**a**) or to the entire cell (ETR_{cell}) (**b**). The measured rates are shown in response to increasing light intensity of *Phaeocystis antarctica* for the Control indicated by cross points, and for the −Mn indicated by circles, while the dotted lines indicate the calculated data from the model.

(Middag et al. 2012; Browning et al. 2014, 2021; Balaguer et al. 2022). Taking these observations together, our *P. antarctica* strain was not limited under the applied low Mn concentrations as naturally occurring in the field.

Still, one must consider that in both Mn-repleted and Mn-depleted treatments, Zn concentrations were 4–60 times higher than the Mn concentrations of the culture medium (Table 1). According to Hawco et al. (2022), Mn limitation might also be tightly related to Zn–Mn interactions in the field, with a higher prevalence of Mn limitation under high Zn concentrations (Hawco et al. 2022). Due to the finding that Zn and Mn compete for the same transporter (Sunda and Huntsman 1998*a*), the possibility that the high Zn concentrations potentially inhibited Mn uptake cannot be excluded from our study. Since we did not observe any differences in terms of growth and POC between the Mn-repleted and Mn-depleted treatments, it seems that the provided Zn supply had no impact and did not promote Mn limitation even in the low Mn treatment, where Zn concentrations were relatively high.

Although studies have investigated Mn limitation in two Antarctic phytoplankton species in the laboratory (Pausch et al. 2019; Wu et al. 2019), information regarding their Mn contents was not incorporated. In our study, with decreasing Mn supply, the Mn : C ratio of the Mn-deficient cells (−Mn) significantly decreased relative to the Control cells (1.7 ± 0.4 and 0.6 ± 0.2 μmol mol^{-1}, respectively; Fig. 2b). As their cellular POC content was not affected by low Mn concentrations relative to FeMn-enriched conditions, this indicates that their internal cellular Mn pool was decreased under low Mn supply. As four Mn ions are needed for the water-splitting complex of photosystem II, a lack of Mn was previously found to disturb the photochemical activity of photosystem II (Peers and Price 2004; Pausch et al. 2019; Wu et al. 2019). Accordingly, the photosynthetic efficiency (F_v/F_m) and recovery values of Mn-deficient *P. antarctica* cells were reduced relative to the Control (Table 2). In addition, *P. antarctica* cells under low Mn supply did not change their functional absorption cross-section of photosystem II (σ_{PSII}) but instead increased both the concentration of functional reaction centers for photosystem II ([RCII]) and fucoxanthin to maximize the capture of light energy (Table 2). Such photoacclimation strategy potentially compensated for the lower efficiency of each photosystem II and was previously suggested for Fe-limited Southern Ocean diatoms and *P. antarctica* (Strzepek et al. 2012), but not yet under low Mn supply. Still, the higher number of photosystem II under the −Mn condition is surprising as additional [RCII] require more Mn, indicating that Mn was possibly relocated from another Mn-dependent metabolic process (e.g., Mn-containing superoxide dismutase, the 2nd most important sink of Mn in the cell; Wolfe-Simon et al. 2005). Consequently, reactive oxygen species production must have been reduced to decrease the need for Mn-containing superoxide dismutase. Reactive oxygen species are formed through leaking electrons generated by photosystem II activity (Asada 2006), which increases when light energy is in excess. Mechanisms such as non-photochemical quenching act as energy dissipaters; however, they were not altered under low Mn supply (Supporting Information Fig. S2). Hence, another alternative pathway to reduce the energy in excess is to have additional RCII. Therefore, Mn may be relocated from the superoxide dismutase to the photosystem II to dissipate the excessive light energy and reduce reactive oxygen species production. In contrast to recovering fewer damaged reaction centers from excess light energy, this pathway may be less energy-expansive.

Surprisingly, POC production rates remained the same while the ETR normalized to photosystem II was reduced in the −Mn treatment compared to the Control treatment (Fig. 3; Table 2). To understand this process, additional cellular modeling simulations were performed (Fig. 4; Supporting Information Table S2). The output of the model indicates that the lowered ETR under low Mn supply cannot be explained by a decrease in pigment concentrations (Supporting Information Table S2), a finding supported by the unaffected LH pigment contents and the increase of fucoxanthin between the −Mn and the Control treatment (Table 3). In addition, the alteration of intrinsic processes in photosystem II (e.g., exciton trapping by open photosystem II and exciton exchange between photosystem II units) due to Mn depletion does not explain the decrease of the ETR (Supporting Information Table S2). Instead, the model simulation reveals that the decreased ETR of the Mn-deficient treatment resulted from a decrease in ferredoxin reduction by photosystem I and/or a decrease of the rate constant for terminal ferredoxin reoxidation at the end of the electron transport chain. Please note that the model cannot differentiate between the latter two processes.

When ferredoxin reduction by photosystem I is only considered, the model shows that the reduced ETR in the −Mn treatment (Fig. 4a) was enhanced by a 25% decrease in the ferredoxin reduction rate (k_{PSI}; Supporting Information Table S2). Henceforth, an upstream process in the electron transport chain behind the Mn-containing photosystem II under low Mn supply may have caused the reduction of ETR. This indicates active downregulation of the electron transport in each photosystem II in Mn-deficient *P. antarctica*. To counteract this, *P. antarctica*, on the other hand, displayed additional RCIIs (Table 2). This strategy was successful as the POC production rate of the −Mn treatment was as high as the Control treatment (Fig. 1c).

The overall ETR of the cell (ETR_{cell}) was calculated to support this finding. The basic assumption that each functional photosystem II has a single RCII (Oxborough 2012) was made, and the ETRs normalized to photosystem II (Fig. 3) were multiplied by the total number of [RCII] (Table 2). Consequently, both Control and −Mn treatments displayed similar ETR_{cell} (Fig. 4b). By having identical ETR_{cell}, the POC production rate of Mn-deficient *P. antarctica* remained unchanged compared

to the Control (Fig. 1c). Hence, through higher RCII abundance, *P. antarctica* maintains stable growth and POC production under low Mn concentrations.

Overall, this study indicates that the growth and POC production of *P. antarctica* was not limited by the naturally low Mn seawater concentrations of our experiments, and this was potentially due to its low Mn requirements.

P. antarctica was limited by low Fe supply

Fe is involved in many metabolic pathways of the cells, such as photosynthesis and respiration processes, nitrogen fixation, and chlorophyll synthesis (Behrenfeld and Milligan 2013; Moore et al. 2013; Twining and Baines 2013). Hence, Fe deficiency in the cells usually leads to a reorganization of the thylakoid membrane. As 23–24 atoms of Fe are needed for photosynthetic electron transport (Raven et al. 1999; Behrenfeld and Milligan 2013), it represents 80% of the total Fe demands. Concomitantly, Fe limitation frequently results in decreased efficiency of electron transport and lower availability of adenosine triphosphate (ATP) and nicotinamide adenine dinucleotide phosphate hydrogen for carbon fixation (Peers and Price 2004). Due to reduced electron transport effectiveness under low Fe supply, growth of *P. antarctica* was reduced in the −Fe treatment compared to the Control (Fig. 1a,c), indicating Fe limitation. A decline in growth rate in response to Fe limitation was already reported for the same (Koch et al. 2019; Trimborn et al. 2019) and other strains of *P. antarctica* (Alderkamp et al. 2012; Rizkallah et al. 2020), also in combination with light (Strzepek et al. 2012, 2019) and Mn (Wu et al. 2019). Fe-limited phytoplankton usually also displays reduced F_v/F_m values and larger σ_{PSII} (Behrenfeld and Kolber 1999; Hopkinson et al. 2007; Trimborn et al. 2015). This strategy applied by our Fe-deficient *P. antarctica* cells (−Fe; Table 2) is known to increase the size of the LH antennas and to reduce the number of Fe-rich photosynthetic reaction centers under Fe-limiting conditions (Strzepek et al. 2012).

Relative to the Control, POC production remained the same under low Fe supply (Fig. 1c). However, the ETR of *P. antarctica* was found to be significantly higher than for the Control (Fig. 3; Table 2), which means that light energy in excess needs to be dissipated via alternative electron pathways, such as the Mehler reaction, where the oxygen is reduced at the acceptor side of photosystem I (Mehler 1951). As previously reported for the Fe-limited diatom *C. debilis* (Pausch et al. 2019), higher ETR coupled with a faster reoxidation time of Q_a (τ_{Qa}; Table 2) indicates a nonreduced state of the plastoquinone pool. In combination with the lower energy exchange between the photosystems (*P*; Table 2), it implies that another pathway was used instead. This alternative channel turns electrons aside after photosystem II oxidation and before photosystem I reduction and would then exclude the possibility of cyclic electron flow within photosystem I (Halsey and Jones 2015). Henceforth, an additional alternative pathway that potentially involves a midstream oxidase, the plastid terminal oxidase (PTOX), which accepts the electrons from the plastoquinone pool to reduce oxygen and regenerate water. By avoiding the Fe-rich photosystem I and cytochrome b6/f (Mackey et al. 2008), this path may sustain ATP production, which appears to be beneficial for some Fe-limited phytoplankton (Mackey et al. 2008; Behrenfeld and Milligan 2013).

The low Fe concentration determined in our −Fe treatment corresponds to values measured in the Ross Sea in December/January (Wu et al. 2019) and the Drake Passage in March (Balaguer et al. 2022), where both the occurrence of *P. antarctica* cells and low dissolved Fe concentrations were simultaneously reported. Under these conditions, the observed lowered growth and photophysiological characteristics suggest that these environments were limiting the −Fe *P. antarctica* cells. Nevertheless, more drastic responses to Fe addition were reported for the same strain of *P. antarctica* (e.g., POC content, Fe : C and F_v/F_m values; Koch et al. 2019) as a result of higher dissolved Fe concentrations applied in their Fe-enriched treatments (4 vs. 2.15 nmol L^{-1} our study). This implies that the Fe-replete treatments in our study were at the border of Fe limitation, and potentially greater Fe effects could have been observed (e.g., on growth and carbon production) if higher Fe concentrations had been applied.

Low FeMn supply mainly provokes physiological characteristics of Fe limitation

Relative to −Fe cells, growth and POC production of FeMn-deficient *P. antarctica* cells remained equally low (Fig. 1a,c). We also observed under low supply of both Fe and Mn (−FeMn) highest ETR together with faster τ_{Qa} relative to −Fe conditions (Tables 2, 3). This indicates photophysiological adjustments of Fe limitation also for the −FeMn treatment. Similar to our −Fe conditions, also under −FeMn conditions, higher PTOX activity potentially enabled the −FeMn-deficient *P. antarctica* cells to yield similar high POC production rates as under low Fe supply alone. Overall, the response of *P. antarctica* under −FeMn is primarily driven by Fe. Similarly, Wu et al. (2019) did not observe changes in the growth of another *P. antarctica* strain between these two treatments (−Fe vs. −FeMn) in a laboratory experiment. The latter, nevertheless, reported significant shifts in flavodoxin and plastocyanin expression patterns of *P. antarctica* when both Fe and Mn concentrations were low relative to low Fe supply alone, indicating FeMn co-limitation. However, a lower light regime was applied compared to ours (25 vs. 100 μmol photons m^{-2} s^{-1} in our study); this potentially enhanced the Mn requirements of *P. antarctica*. Under low light intensities, LH pigment production must be increased, thereby enhancing Fe requirements (Sunda and Huntsman 1998*b*; Strzepek and Price 2000). Some Southern Ocean phytoplankton species possess adaptative mechanisms to cope with low Fe-light environments, including acclimation strategies to keep cellular Fe requirements constant (Strzepek et al. 2012). Nonetheless,

little is known about the additional effects of Mn limitation under varying light supply. Henceforth, light limitation may strengthen the interdependence of Fe and Mn and enhance the production of reactive oxygen species (Peers and Price 2004; McCain et al. 2021).

Ecological implications

Our study, together with another laboratory (Pausch et al. 2019; Wu et al. 2019) and field studies (Browning et al. 2014, 2021; Balaguer et al. 2022), pinpoint the need to investigate species-specific requirements for Fe and Mn to be able to better understand Southern Ocean phytoplankton community structure. This study reveals that different from the Southern Ocean diatoms *C. debilis* (Pausch et al. 2019) and *Fragilaropsis* sp. (Balaguer et al. 2022), the solitary *P. antarctica* possessed the capacity to cope well with low Mn seawater concentrations. In Fe-limited open ocean waters, where solitary cells of *P. antarctica* mostly thrive (Smith et al. 2003), future climate change scenarios predict a deepening of the upper mixed water layer (Hauck et al. 2015) induced by stronger westerly winds (Meijers 2014). The consequence of this physical forcing would inject additional Mn into Southern Ocean surface waters. One could speculate that diatoms (such as *C. debilis* [Pausch et al. 2019] or *Fragilariopsis* sp. [Balaguer et al. 2022]) will potentially benefit from the Mn release, whereas single-celled haptophytes like *P. antarctica* may not. However, a deepening of the mixed water layer would reduce light availability in the upper surface layer and may affect its Mn requirements, as revealed with *P. antarctica* populations of the Ross Sea (Wu et al. 2019). Currently, the influence of light availability with low Mn concentrations remains poorly understood. At least under low Fe conditions, it is known that the Mn requirement increases (Peers and Price 2004), but how this affects the physiology of Southern Ocean phytoplankton species is yet not comprehended in the context of low Mn supply. Irrespective of the future climate scenarios, our study reveals that different from diatoms, *P. antarctica* displays efficient physiological strategies to cope with low Mn supply. The response to the limitation of varying trace metals between different phytoplankton groups can have significant consequences, on which phytoplankton species potentially dominate blooms and therefore influence the efficiency of the biological carbon pump.

Data availability statement

All data needed to evaluate the conclusions in the paper are present in the paper and/or Supporting Information Materials. Additional data are freely available from the PANGAEA data repository (https://doi.org/10.1594/PANGAEA.944462).

References

Alderkamp, A.-C., G. Kulk, A. G. Buma, R. J. Visser, G. L. Van Dijken, M. M. Mills, and K. R. Arrigo. 2012. The effect of iron limitation on the photophysiology of *Phaeocystis antarctica* (prymnesiophyceae) and *Fragilariopsis cylindrus* (bacillariophyceae) under dynamic irradiance. J. Phycol. **48**: 45–59. doi:10.1111/j.1529-8817.2011.01098.x

Asada, K. 2006. Production and scavenging of reactive oxygen species in chloroplasts and their functions. Plant Physiol. **141**: 391–396. doi:10.1104/pp.106.082040

Balaguer, J., F. Koch, C. Hassler, and S. Trimborn. 2022. Iron and manganese co-limit the growth of two phytoplankton groups dominant at two locations of the Drake Passage. Commun. Biol. **5**: 207. doi:10.1038/s42003-022-03148-8

Behrenfeld, M. J., and Z. S. Kolber. 1999. Widespread iron limitation of phytoplankton in the South Pacific Ocean. Science **283**: 840–843. doi:10.1126/science.283.5403.840

Behrenfeld, M. J., and A. J. Milligan. 2013. Photophysiological expressions of iron stress in phytoplankton. Ann. Rev. Mar. Sci. **5**: 217–246. doi:10.1146/annurev-marine-121211-172356

Biller, D. V., and K. W. Bruland. 2012. Analysis of Mn, Fe, Co, Ni, Cu, Zn, Cd, and Pb in seawater using the Nobias-chelate PA1 resin and magnetic sector inductively coupled plasma mass spectrometry (ICP-MS). Mar. Chem. **130**: 12–20. doi:10.1016/j.marchem.2011.12.001

Boyd, P. W., and others. 2007. Mesoscale iron enrichment experiments 1993-2005: Synthesis and future directions. Science **315**: 612–617. doi:10.1126/science.1131669

Browning, T. J., H. A. Bouman, G. M. Henderson, T. A. Mather, D. M. Pyle, C. Schlosser, E. M. S. Woodward, and C. M. Moore. 2014. Strong responses of Southern Ocean phytoplankton communities to volcanic ash. Geophys. Res. Lett. **41**: 2851–2857. doi:10.1002/2014GL059364

Browning, T. J., E. P. Achterberg, A. Engel, and E. Mawji. 2021. Manganese co-limitation of phytoplankton growth and major nutrient drawdown in the Southern Ocean. Nat. Commun. **12**: 884. doi:10.1038/s41467-021-21122-6

Buma, A. G., H. J. de Baar, R. F. Nolting, and A. J. van Bennekom. 1991. Metal enrichment experiments in the Weddell-Scotia Seas: Effects of iron and manganese on various plankton communities. Limnol. Oceanogr. **36**: 1865–1878. doi:10.4319/lo.1991.36.8.1865

DiTullio, G. R., and others. 2000. Rapid and early export of *Phaeocystis antarctica* blooms in the Ross Sea, Antarctica. Nature **404**: 595–598. doi:10.1038/35007061

DiTullio, G. R., N. Garcia, S. F. Riseman, and P. N. Sedwick. 2007. Effects of iron concentration on pigment composition in *Phaeocystis antarctica* grown at low irradiance, p. 71–81. *In* M. A. van Leeuwe, J. Stefels, S. Belviso, C. Lancelot, P. G. Verity, and W. W. C. Gieskes [eds.], Phaeocystis, major link in the biogeochemical cycling of climate-relevant elements. Springer. doi:10.1007/978-1-4020-6214-8_7

El-Sayed, S. Z., D. C. Biggs, and O. Holm-Hansen. 1983. Phytoplankton standing crop, primary productivity, and near-surface nitrogenous nutrient fields in the Ross Sea,

Antarctica. Deep-Sea Res. A: Oceanogr. Res. Pap. **30**: 871–886. doi:10.1016/0198-0149(83)90005-5

Gerringa, L. J. A., H. J. W. de Baar, and K. R. Timmermans. 2000. A comparison of iron limitation of phytoplankton in natural oceanic waters and laboratory media conditioned with EDTA. Mar. Chem. **68**: 335–346. doi:10.1016/S0304-4203(99)00092-4

Guillard, R. R., and J. H. Ryther. 1962. Studies of marine planktonic diatoms: I. *Cyclotella nana* Hustedt, and *Detonula confervacea* (Cleve) Gran. Can. J. Microbiol. **8**: 229–239. doi:10.1139/m62-029

Halsey, K. H., and B. M. Jones. 2015. Phytoplankton strategies for photosynthetic energy allocation. Ann. Rev. Mar. Sci. **7**: 265–297. doi:10.1146/annurev-marine-010814-015813

Hassler, C. S., and V. Schoemann. 2009. Discriminating between intra-and extracellular metals using chemical extractions: An update on the case of iron. Limnol. Oceanogr.: Methods **7**: 479–489. doi:10.4319/lom.2009.7.479

Hathorne, E. C., B. Haley, T. Stichel, P. Grasse, M. Zieringer, and M. Frank. 2012. Online preconcentration ICP-MS analysis of rare earth elements in seawater. Geochem. Geophys. Geosyst. **13**: 1–12. doi:10.1029/2011GC003907

Hauck, J., and others. 2015. On the Southern Ocean CO_2 uptake and the role of the biological carbon pump in the 21st century. Glob. Biogeochem. Cycles **29**: 1451–1470. doi:10.1002/2015GB005140

Hawco, N. J., A. Tagliabue, and B. S. Twining. 2022. Manganese limitation of phytoplankton physiology and productivity in the Southern Ocean. Glob. Biogeochem. Cycles **36**: e2022GB007382. doi:10.1029/2022GB007382

Ho, T.-Y., A. Quigg, Z. V. Finkel, A. J. Milligan, K. Wyman, P. G. Falkowski, and F. M. M. Morel. 2003. The elemental composition of some marine phytoplankton. Journal of Phycology, **39**: 1145–1159. https://doi.org/10.1111/j.0022-3646.2003.03-090.x

Hopkinson, B. M., and others. 2007. Iron limitation across chlorophyll gradients in the southern Drake Passage: Phytoplankton responses to iron addition and photosynthetic indicators of iron stress. Limnol. Oceanogr. **52**: 2540–2554. doi:10.4319/lo.2007.52.6.2540

Koch, F., S. Beszteri, L. Harms, and S. Trimborn. 2019. The impacts of iron limitation and ocean acidification on the cellular stoichiometry, photophysiology, and transcriptome of *Phaeocystis antarctica*. Limnol. Oceanogr. **64**: 357–375. doi:10.1002/lno.11045

Kroon, B. M. A., and S. Thoms. 2006. From electron to biomass: A mechanistic model to describe phytoplankton photosynthesis and steady-state growth rates. J. Phycol. **42**: 593–609. doi:10.1111/j.1529-8817.2006.00221.x

Lancelot, C., P. Wassmann, and H. Barth. 1994. Ecology of *Phaeocystis*-dominated ecosystems. J. Mar. Syst. **5**: 1–4. doi:10.1016/0924-7963(94)90012-4

Mackey, K. R., A. Paytan, A. R. Grossman, and S. Bailey. 2008. A photosynthetic strategy for coping in a high-light, low-nutrient environment. Limnol. Oceanogr. **53**: 900–913. doi:10.4319/lo.2008.53.3.0900

Martin, J. H., S. E. Fitzwater, and R. M. Gordon. 1990*a*. Iron deficiency limits phytoplankton growth in Antarctic waters. Glob. Biogeochem. Cycles **4**: 5–12. doi:10.1029/GB004i001p00005

Martin, J. H., R. M. Gordon, and S. E. Fitzwater. 1990*b*. Iron in Antarctic waters. Nature **345**: 156–158. doi:10.1038/345156a0

McCain, J. S. P., A. Tagliabue, E. Susko, E. P. Achterberg, A. E. Allen, and E. M. Bertrand. 2021. Cellular costs underpin micronutrient limitation in phytoplankton. Sci. Adv. **7**: eabg6501. doi:10.1126/sciadv.abg6501

Mehler, A. H. 1951. Studies on reactions of illuminated chloroplasts: I. Mechanism of the reduction of oxygen and other hill reagents. Arch. Biochem. Biophys. **33**: 65–77. doi:10.1016/0003-9861(51)90082-3

Meijers, A. J. S. 2014. The Southern Ocean in the coupled model intercomparison project phase 5. Philos. Trans. A Math. Phys. Eng. Sci. **372**: 20130296. doi:10.1098/rsta.2013.0296

Middag, R., H. J. W. de Baar, P. Laan, P. H. Cai, and J. C. van Ooijen. 2011. Dissolved manganese in the Atlantic sector of the Southern Ocean. Deep-Sea Res. II: Top. Stud. Oceanogr. **58**: 2661–2677. doi:10.1016/j.dsr2.2010.10.043

Middag, R., H. J. W. de Baar, P. Laan, and O. Huhn. 2012. The effects of continental margins and water mass circulation on the distribution of dissolved aluminum and manganese in Drake Passage. J. Geophys. Res.: Oceans **117**: C01019. doi:10.1029/2011JC007434

Middag, R., H. J. de Baar, M. B. Klunder, and P. Laan. 2013. Fluxes of dissolved aluminum and manganese to the Weddell Sea and indications for manganese co-limitation. Limnol. Oceanogr. **58**: 287–300. doi:10.4319/lo.2013.58.1.0287

Moore, C. M., and others. 2013. Processes and patterns of oceanic nutrient limitation. Nat. Geosci. **6**: 701–710. doi:10.1038/ngeo1765

Oxborough, K. 2012. FastPro8 GUI and FRRf3 systems documentation. Chelsea Technologies Group Ltd.

Oxborough, K., and N. R. Baker. 1997. Resolving chlorophyll *a* fluorescence images of photosynthetic efficiency into photochemical and non-photochemical components—calculation of qP and Fv-/Fm-; without measuring Fo. Photosynth. Res. **54**: 135–142. doi:10.1023/A:1005936823310

Oxborough, K., C. M. Moore, D. J. Suggett, T. Lawson, H. G. Chan, and R. J. Geider. 2012. Direct estimation of functional PSII reaction center concentration and PSII electron flux on a volume basis: A new approach to the analysis of fast repetition rate fluorometry (FRRf) data. Limnol. Oceanogr.: Methods **10**: 142–154. doi:10.4319/lom.2012.10.142

Pausch, F., K. Bischof, and S. Trimborn. 2019. Iron and manganese co-limit growth of the Southern Ocean diatom

Chaetoceros debilis. PloS One **14**: e0221959. doi:10.1371/journal.pone.0221959

Peers, G., and N. M. Price. 2004. A role for manganese in superoxide dismutases and growth of iron-deficient diatoms. Limnol. Oceanogr. **49**: 1774–1783. doi:10.4319/lo.2004.49.5.1774

Platt, T., C. L. Gallegos, and W. G. Harrison. 1981. Photoinhibition of photosynthesis in natural assemblages of marine phytoplankton.

Rapp, I., C. Schlosser, D. Rusiecka, M. Gledhill, and E. P. Achterberg. 2017. Automated preconcentration of Fe, Zn, Cu, Ni, Cd, Pb, Co, and Mn in seawater with analysis using high-resolution sector field inductively-coupled plasma mass spectrometry. Anal. Chim. Acta **976**: 1–13. doi:10.1016/j.aca.2017.05.008

Raven, J. A. 1990. Predictions of Mn and Fe use efficiencies of phototrophic growth as a function of light availability for growth and of C assimilation pathway. New Phytol. **116**: 1–18. doi:10.1111/j.1469-8137.1990.tb00505.x

Raven, J. A., M. C. Evans, and R. E. Korb. 1999. The role of trace metals in photosynthetic electron transport in O_2-evolving organisms. Photosynth. Res. **60**: 111–150. doi:10.1023/A:1006282714942

Rizkallah, M. R., S. Frickenhaus, S. Trimborn, L. Harms, A. Moustafa, V. Benes, S. Gäbler-Schwarz, and S. Beszteri. 2020. Deciphering patterns of adaptation and acclimation in the transcriptome of *Phaeocystis antarctica* to changing iron conditions. J. Phycol. **56**: 747–760. doi:10.1111/jpy.12979

Schoemann, V., S. Becquevort, J. Stefels, V. Rousseau, and C. Lancelot. 2005. *Phaeocystis* blooms in the global ocean and their controlling mechanisms: A review. J. Sea Res. **53**: 43–66. doi:10.1016/j.seares.2004.01.008

Silsbe, G. M., and J. C. Kromkamp. 2012. Modeling the irradiance dependency of the quantum efficiency of photosynthesis. Limnol. Oceanogr.: Methods **10**: 645–652. doi:10.4319/lom.2012.10.645

Smith, W. O., M. R. Dennett, S. Mathot, and D. A. Caron. 2003. The temporal dynamics of the flagellated and colonial stages of *Phaeocystis antarctica* in the Ross Sea. Deep-Sea Res. II: Top. Stud. Oceanogr. **50**: 605–617. doi:10.1016/S0967-0645(02)00586-6

Stoecker, D. K., M. Putt, and T. Moisan. 1995. Nano-and microplankton dynamics during the spring *Phaeocystis* sp. bloom in McMurdo Sound, Antarctica. J. Mar. Biol. Assoc. UK **75**: 815–832. doi:10.1017/S0025315400038170

Strzepek, R. F., and N. M. Price. 2000. Influence of irradiance and temperature on the iron content of the marine diatom *Thalassiosira weissflogii* (Bacillariophyceae). Mar. Ecol. Prog. Ser. **206**: 107–117. doi:10.3354/meps206107

Strzepek, R. F., K. A. Hunter, R. D. Frew, P. J. Harrison, and P. W. Boyd. 2012. Iron-light interactions differ in Southern Ocean phytoplankton. Limnol. Oceanogr. **57**: 1182–1200. doi:10.4319/lo.2012.57.4.1182

Strzepek, R. F., P. W. Boyd, and W. G. Sunda. 2019. Photosynthetic adaptation to low iron, light, and temperature in Southern Ocean phytoplankton. Proc. Natl. Acad. Sci. USA **116**: 4388–4393. doi:10.1073/pnas.1810886116

Suggett, D. J., H. L. MacIntyre, and R. J. Geider. 2004. Evaluation of biophysical and optical determinations of light absorption by photosystem II in phytoplankton. Limnol. Oceanogr.: Methods **2**: 316–332. doi:10.4319/lom.2004.2.316

Suggett, D. J., C. M. Moore, A. E. Hickman, and R. J. Geider. 2009. Interpretation of fast repetition rate (FRR) fluorescence: Signatures of phytoplankton community structure versus physiological state. Mar. Ecol. Prog. Ser. **376**: 1–19. doi:10.3354/meps07830

Sunda, W. 2012. Feedback interactions between trace metal nutrients and phytoplankton in the ocean. Front. Microbiol. **3**: 204. doi:10.3389/fmicb.2012.00204

Sunda, W. G., and S. A. Huntsman. 1983. Effect of competitive interactions between manganese and copper on cellular manganese and growth in estuarine and oceanic species of the diatom Thalassiosira. Limnol. Oceanogr. **28**: 924–934. doi:10.4319/lo.1983.28.5.0924

Sunda, W. G., and S. A. Huntsman. 1998*a*. Interactions among Cu^{2+}, Zn^{2+}, and Mn^{2+} in controlling cellular Mn, Zn, and growth rate in the coastal alga *Chlamydomonas*. Limnol. Oceanogr. **43**: 1055–1064. doi:10.4319/lo.1998.43.6.1055

Sunda, W. G., and S. A. Huntsman. 1998*b*. Processes regulating cellular metal accumulation and physiological effects: Phytoplankton as model systems. Sci. Total Environ. **219**: 165–181. doi:10.1016/S0048-9697(98)00226-5

Trimborn, S., C. J. Hoppe, B. B. Taylor, A. Bracher, and C. Hassler. 2015. Physiological characteristics of open ocean and coastal phytoplankton communities of Western Antarctic Peninsula and Drake Passage waters. Deep-Sea Res. I: Oceanogr. Res. Pap. **98**: 115–124. doi:10.1016/j.dsr.2014.12.010

Trimborn, S., S. Thoms, K. Bischof, and S. Beszteri. 2019. Susceptibility of two Southern Ocean phytoplankton key species to iron limitation and high light. Front. Mar. Sci. **6**: 167. doi:10.3389/fmars.2019.00167

Twining, B. S., and S. B. Baines. 2013. The trace metal composition of marine phytoplankton. Ann. Rev. Mar. Sci. **5**: 191–215. doi:10.1146/annurev-marine-121211-172322

Utermöhl, H. 1958. Zur vervollkommnung der quantitativen phytoplankton-methodik: Mit 1 Tabelle und 15 abbildungen im Text und auf 1 Tafel. Mitt. Int. Ver. Theor. Angew. Limnol. **9**: 1–38. doi:10.1080/05384680.1958.11904091

van Leeuwe, M. A., and J. Stefels. 1998. Effects of iron and light stress on the biochemical composition of Antarctic *Phaeocystis* sp. (Prymnesiophyceae). II. Pigment composition. J. Phycol. **34**: 496–503. doi:10.1046/j.1529-8817.1998.340496.x

van Leeuwe, M. A., and J. Stefels. 2007. Photosynthetic responses in *Phaeocystis antarctica* towards varying light and iron conditions, p. 61–70. *In* M. A. van Leeuwe, J. Stefels, S.

Belviso, C. Lancelot, P. G. Verity, and W. W. C. Gieskes [eds.], Phaeocystis, major link in the biogeochemical cycling of climate-relevant elements. Springer. doi:10.1007/978-1-4020-6214-8_6

Wolfe-Simon, F., D. Grzebyk, O. Schofield, and P. G. Falkowski. 2005. The role and evolution of superoxide dismutases in algae. J. Phycol. **41**: 453–465. doi:10.1111/j.1529-8817.2005.00086.x

Wright, S. W., S. W. Jeffrey, R. F. C. Mantoura, C. A. Llewellyn, T. Bjørnland, D. Repeta, and N. Welschmeyer. 1991. Improved HPLC method for the analysis of chlorophylls and carotenoids from marine phytoplankton. Mar. Ecol. Prog. Ser. **77**: 183–196. doi:10.3354/meps077183

Wu, M., J. S. P. McCain, E. Rowland, R. Middag, M. Sandgren, A. E. Allen, and E. M. Bertrand. 2019. Manganese and iron deficiency in Southern Ocean *Phaeocystis antarctica* populations revealed through taxon-specific protein indicators. Nat. Commun. **10**: 3582. doi:10.1038/s41467-019-11426-z

Yu, Q., and Z. Rengel. 1999. Micronutrient deficiency influences plant growth and activities of superoxide dismutases in narrow-leafed lupins. Ann. Bot. **83**: 175–182. doi:10.1006/anbo.1998.0811

Acknowledgments

J.B. was funded by the Deutsche Forschungsgemeinschaft (DFG) in the framework of the priority program "Antarctic Research with comparative investigations in Arctic ice areas," project TR 899/4-1. In addition, we would like to thank Kai Bischof and Britta Meyer-Schlosser for the pigment analysis, Kristof Möller and Henning Hellmer for the support in the laboratory, and Christian Völkner for the dissolved and intracellular Fe and Mn analysis. Open Access funding enabled and organized by Projekt DEAL.

Conflict of Interest

None declared.

Submitted 02 September 2022
Revised 04 July 2023
Accepted 15 July 2023

Associate editor: Jana Hinners